Differential Diagnosis in Neuroimaging: Brain and Meninges

Steven P. Meyers

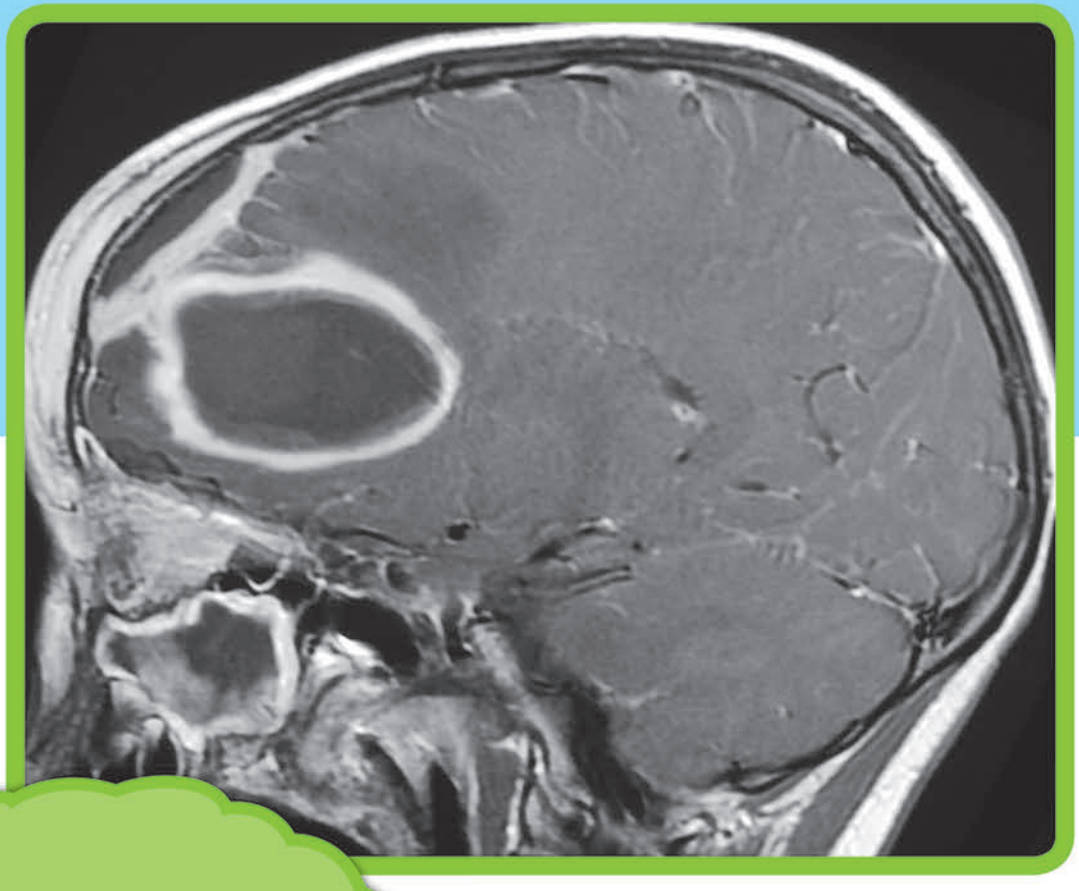

Thieme


Thieme

Differential Diagnosis in Neuroimaging

Brain and Meninges

Steven P. Meyers, MD, PhD, FACR
Professor of Radiology/Imaging Sciences, Neurosurgery, and Otolaryngology
Director, Radiology Residency Program
University of Rochester School of Medicine and Dentistry
Rochester, New York

1952 illustrations

Thieme
New York • Stuttgart • Delhi • Rio de Janeiro

Executive Editor: William Lamsback
Managing Editor: J. Owen Zurhellen IV
Director, Editorial Services: Mary Jo Casey
Editorial Consultant: Judith Tomat
Production Editor: Kenneth L. Chumbley
International Production Director: Andreas Schabert
Vice President, Editorial and E-Product Development: Vera Spillner
International Marketing Director: Fiona Henderson
International Sales Director: Louisa Turrell
Director of Sales, North America: Mike Roseman
Senior Vice President and Chief Operating Officer: Sarah Vanderbilt
President: Brian D. Scanlan

Library of Congress Cataloging-in-Publication Data

Names: Meyers, Steven P., author.
Title: Differential diagnosis in neuroimaging. Brain and meninges / Steven P. Meyers.
Description: New York : Thieme, [2016] | Includes bibliographical references.
Identifiers: LCCN 2016013145 | ISBN 9781604067002 (alk. paper) | ISBN 9781604067026 (eISBN)
Subjects: | MESH: Neuroimaging | Brain Diseases—diagnosis | Magnetic Resonance Imaging | Diagnosis, Differential
Classification: LCC RC349.D52 | NLM WL 141.5.N47 | DDC 616.8/04754—dc23
LC record available at https://lccn.loc.gov/2016013145

Important note: Medicine is an ever-changing science undergoing continual development. Research and clinical experience are continually expanding our knowledge, in particular our knowledge of proper treatment and drug therapy. Insofar as this book mentions any dosage or application, readers may rest assured that the authors, editors, and publishers have made every effort to ensure that such references are in accordance with **the state of knowledge at the time of production of the book.**

Nevertheless, this does not involve, imply, or express any guarantee or responsibility on the part of the publishers in respect to any dosage instructions and forms of applications stated in the book. **Every user is requested to examine carefully** the manufacturers' leaflets accompanying each drug and to check, if necessary in consultation with a physician or specialist, whether the dosage schedules mentioned therein or the contraindications stated by the manufacturers differ from the statements made in the present book. Such examination is particularly important with drugs that are either rarely used or have been newly released on the market. Every dosage schedule or every form of application used is entirely at the user's own risk and responsibility. The authors and publishers request every user to report to the publishers any discrepancies or inaccuracies noticed. If errors in this work are found after publication, errata will be posted at www.thieme.com on the product description page.

Some of the product names, patents, and registered designs referred to in this book are in fact registered trademarks or proprietary names even though specific reference to this fact is not always made in the text. Therefore, the appearance of a name without designation as proprietary is not to be construed as a representation by the publisher that it is in the public domain.

Thieme Publishers New York
333 Seventh Avenue, New York, NY 10001 USA
+1 800 782 3488, customerservice@thieme.com

Thieme Publishers Stuttgart
Rüdigerstrasse 14, 70469 Stuttgart, Germany
+49 [0]711 8931 421, customerservice@thieme.de

Thieme Publishers Delhi
A-12, Second Floor, Sector-2, Noida-201301
Uttar Pradesh, India
+91 120 45 566 00, customerservice@thieme.in

Thieme Publishers Rio de Janeiro, Thieme Publicações Ltda.
Edifício Rodolpho de Paoli, 25º andar
Av. Nilo Peçanha, 50 – Sala 2508
Rio de Janeiro 20020-906, Brasil
+55 21 3172 2297

Cover design: Thieme Publishing Group
Typesetting by Prairie Papers

Printed in China by Asia Pacific Offset 5 4 3 2 1

ISBN 978-1-60406-700-2

Also available as an e-book:
eISBN 978-1-60406-702-6

To my parents, for their unwavering encouragement and support along my long journey through formal education.

And to my wife, Barbara, and son, Noah, for their continuous love, support, and patience during this project.

Contents

Preface

As an academic neuroradiologist who has had the privilege of working at a university medical center for the past twenty-five years, I have had many opportunities to continuously learn and be involved in the education of medical students, as well as residents and fellows in radiology, neurosurgery, neurology, otolaryngology, and orthopedics. During my training, I had the opportunity to work with outstanding professors who served as role models for teaching and research. I learned from them that excellent teaching cases are invaluable in the education of our specialty. For the past three decades, I have been collecting and organizing a large teaching file for lectures, as well as an educational resource that can be utilized at the workstation. It is from this large data base that I began writing this three-volume series in my specialty of neuroradiology ten years ago.

The goal of these books is to present the imaging features of neuroradiological abnormalities in an easy-to-use resource, with extensive utilization of figures for illustration. This first volume of the series—*Differential Diagnosis in Neuroimaging: Brain and Meninges*—covers lesions involving the brain, ventricles, meninges, and neurovascular system in both children and adults.

The second volume of this series—*Differential Diagnosis in Neuroimaging: Head and Neck*—contains chapters describing lesions located in the skull and temporal bone, orbits, paranasal sinuses and nasal cavity, suprahyoid neck, infrahyoid neck, and brachial plexus.

The third volume—*Differential Diagnosis in Neuroimaging: Spine*—includes differential diagnosis tables, such as congenital and developmental abnormalities, intradural intramedullary lesions (spinal cord lesions), dural and intradural extramedullary lesions, extradural lesions, solitary osseous lesions involving the spine, multifocal lesions and/or poorly-defined signal abnormalities involving the spine, traumatic lesions, and lesions involving the sacrum.

The organization of these books focuses on lists of differential diagnoses of lesions based on anatomic locations in a tabular format. Brief introductory summaries with illustrations are provided at the beginning of most chapters to succinctly provide relevant information, after which the tables are presented. Each of the lesions listed in the tables has a column summarizing the pertinent Imaging findings associated with images for illustration, and a Comments column summarizing key clinical data. References are provided in alphabetical order at the end of each chapter. For the reader's convenience, some of the diagnoses are listed in two or more tables. The purpose of this is to minimize or eliminate the need to page back to the same entries in other tables in order to find the desired information.

These books' unique organization helps the reader obtain information efficiently and quickly. Because of the heavy emphasis on providing illustrative images over text, this book's format can be an effective guide in narrowing the differential diagnoses of lesions based on their locations and imaging findings.

I hope these texts will be a valuable resource for practicing radiologists, neurosurgeons, neurologists, otolaryngologists, and orthopedic spine surgeons. They are intended to become a "well-thumbed text" at the PACS station and clinics. They should also serve as a useful review and teaching guide for trainees in radiology, neurosurgery, neurology, orthopedics, otolaryngology, and other medical specialties preparing for board examinations.

Steven P. Meyers, MD, PhD, FACR

Acknowledgments

I wish to acknowledge the Thieme staff, in particular J. Owen Zurhellen IV, Judith Tomat, William Lamsback, and Kenny Chumbley, for their dedication, hard work, and attention to detail. I thank Ms. Colleen Cottrell for her outstanding secretarial work with this project. I also thank Nadezhda D. Kiriyak, BFA, and Katie Tower, BFA, for their creative talents in making illustrations for this book. I thank Sarah Klingenberger and Margaret Kowaluk for helping me optimize the MRI and CT images of this book.

In addition, I wish to acknowledge the following for their contribution of interesting cases: Jeevak Almast, MBBS, Allan Bernstein, MD, Gary M. Hollenberg, MD, Edward Lin, MD, BBA, Michael Potchen, MD, Peter Rosella, MD, David Shrier, MD, Eric P. Weinberg, MD, and Andrea Zynda-Weiss, MD.

I extend my appreciation and thanks to my coworkers and physician colleagues (Drs. Bernstein, Hollenberg, Rosella, Shrier, Weinberg, and Zynda-Weiss) at University Medical Imaging, the Outpatient Diagnostic Imaging Facility of the University of Rochester, for making an ideal collaborative environment for teaching and clinical service.

Last, I would like to give thanks to my former teachers and mentors for their guidance, encouragement, and friendship.

Illustrations by:

Katie Tower, Figs. 1.1, 1.2, 1.3, 1.4, 1.5, 1.408, 4.1, 5.3, 5.6, 5.9, 5.10, 5.12, 5.13, 5.19

Nadezhda D. Kiriyak, Figs. 1.6, 5.1

Abbreviations

ACA Anterior cerebral artery

ACOM Anterior communicating artery

ADC Apparent diffusion coefficent

ADEM Acute disseminated encephalomyelitis

AML Acute myelogenous leukemia

ANA Antinuclear antibodies

AP Anteroposterior

AS Ankylosing spondylitis

AT/RT Atypical teratoid/rhabdoid tumor

AVF Arteriovenous fistula

AVM Arteriovenous malformation

Ca Calcium/calcification

CADASIL Cerebral autosomal dominant arteriopathy with subcortical infarcts and leukoencephalopathy

CARASIL Cerebral autosomal recessive arteriopathy with subcortical infarcts and leukoencephalopathy

Cho Choline

CISS Constructive interference steady state

CLL Chronic lymphocytic leukemia

CML Chronic myelogenous leukemia

CMV Human cytomegalovirus

CNS Central nervous system

CPPD Calcium pyrophosphate dihydrate deposition

CSF Cerebrospinal fluid

CT Computed tomography

DISH Diffuse idiopathic skeletal hyperostosis

DNET Dysembryoplastic neuroectodermal tumor

DTI Diffusion tensor imaging

DWI Diffusion weighted imaging

EG Eosinophilic granuloma

EMA Epithelial membrane antigen

FIESTA Fast imaging employing steady state acquisition

FLAIR Fluid attenuation inversion recovery

FS Frequency selective fat signal suppression

FSE Fast spin echo

FS-PDWI Fat-suppressed proton density weighted imaging

FSPGR Fast spoiled gradient echo Imaging

FS-T1WI Fat-suppressed T1-weighted imaging

FS-T2WI Fat-suppressed T2-weighted imaging

Gd-contrast Gadolinium-chelate contrast

GRE Gradient echo imaging

HIV Human immundeficiency virus

HMB-45 Human melanoma black monoclonal antibody

HPF High power field

HPV Human papilloma virus

HSV Herpes simplex virus

HU Hounsfield unit

ICA Internal carotid artery

IRIS Immune reconstitution inflammatory syndrome

JIA Juvenile idiopathic arthritis

LCH Langerhans cell histiocytosis

MCA Middle cerebral artery

MDS Myelodysplastic syndrome

MELAS Mitochondrial encephalopathy, lactic acidosis, and stroke-like events

MERRF Myoclonic epilepsy with ragged red fibers

MIP Maximum intensity projection

MPNST Malignant peripheral nerve sheath tumor

MRA MR angiography

MRV MR venography

MRS MR spectroscopy

MS Multiple Sclerosis

NAA N-acetylaspartate

NF1 Neurofibromatosis Type 1

NF2 Neurofibromatosis Type 2

NSAID Non-steroidal anti-inflammatory drug

NSE Neuron specific enloase

PC Phase contrast

PCA Posterior cerebral artery

PCV Polycythemia vera

PCOM Posterior communicating artery

PDWI Proton density weighted imaging

PEDD Proton-electron dipole-dipole interaction

PML Progressive multifocal leukoencephalopathy

PNET Primitive neuroectodermal tumor

PRES Posterior reversible encephalopathy syndrome

PVNS Pigmented villondular synovitis

RF Radiofrequency

SLE Systemic lupus erythematosus

SMA Smooth muscle actin antibodies

STIR Short TI inversion recovery imaging

SWI Susceptibility weighted imaging

S-100 Cellular calcium binding protein in cytoplasm and/or nuceus

T1 Spin-lattice or longitudinal relaxation time (coefficient)

T2 Spin-spin or transverse relaxation time (coefficient)

T2* Effective spin-spin relaxation time using GRE pulse sequence

T2-PRE T2-proton relaxation enhancement

T1WI T1-weighted imaging

T2WI T2-weighted imaging

TE Time to echo

TR Pulse repetition time interval

TOF Time of flight

2D 2 Dimensional

3D 3 Dimensional

WHO World Health Organization

Prologue

Intracranial Abnormalities

Brain, Ventricles, Meninges, Skull, and Vascular Structures

Major advantages of magnetic resonance imaging (MRI) include excellent soft tissue contrast resolution, multiplanar imaging capabilities, dynamic rapid data acquisition, and the available contrast agents. MRI has proven to be a powerful imaging modality in the evaluation of congenital anomalies of the brain; disorders of histogenesis; neoplasms of the central nervous system, cranial nerves, pituitary gland, meninges, and skull base; traumatic lesions; intracranial hemorrhage; ischemia and infarction; infectious and noninfectious diseases; metabolic disorders; and dysmyelinating and demyelinating diseases.

Computed tomography (CT) has been used in the evaluation of neoplasms of the central nervous system, meninges, calvarium, and skull base; traumatic lesions; intracranial hemorrhage; ischemia and infarction (particularly using CT perfusion studies); infectious and noninfectious diseases; and metabolic disorders. Because of its widespread availability and rapid imaging capability, CT plays an important role in the evaluation of acutely injured patients in emergency departments. Multidetector CT is an excellent imaging modality for evaluation of the skull base, orbits, nasopharynx, oropharynx, and floor of the mouth. CT is a useful method for imaging the location and extent of osseous lesions at the skull base, such as metastatic tumors, myeloma, chordomas, and chondrosarcomas.

MRI and CT data can also be used to generate images of arteries and veins (MR angiography and CT angiography) in displays similar to conventional angiography. Other options with clinical MRI scanners include the acquisition of spectral data to characterize the biochemical properties of selected regions of interest in the brain (magnetic resonance spectroscopy), detection of water proton diffusion in brain and meninges (diffusion-weighted imaging and mapping of apparent diffusion coefficients), and evaluation of differing ratios of deoxyhemoglobin to oxyhemoglobin at sites of brain activation (functional MRI).

Appearance of Normal Brain Tissue on CT and MRI

The appearance of brain tissue depends on the CT technique and MRI pulse sequences used, as well as the age of the patient. Myelination of the brain begins in the fifth fetal month and progresses rapidly during the first 2 years of life. The degree of myelination affects the appearance of the brain parenchyma on MRI and CT. In adults, the cerebral cortex has an intermediate signal on T1-weighted images and is lower or hypointense relative to normal white matter. On T2-weighted images, gray matter has an intermediate signal that is higher in signal (hyperintense) relative to white matter. For infants less than 6 months old, the MRI pattern is reversed due to the immature myelination of their brain tissue. Maturation or myelination of the brain tissue, as seen on T1-weighted versus T2-weighted images, occurs at different rates. The myelination proceeds in a predictable and characteristic pattern with regard to location and timing. The changes on T1-weighted images become most evident during the first 6 months of postnatal life, whereas the changes on T2-weighted images are most apparent from 6 to 18 months. At around 6 months of age, the adult MRI signal pattern of the gray and white matter begins to progressively emerge. After 18 months, the brain has a mature MRI appearance with regard to the gray and white matter signal patterns.

On CT, the appearance of brain tissue depends on the mAs and kVp used. Immature myelin in neonates and infants has lower attenuation than myelin in older children. In adults, the cerebral cortex has an intermediate attenuation that is slightly higher relative to normal white matter. The imaging changes seen with myelin maturation are more optimally seen with MRI than with CT.

In addition to the commonly used standard fast spin echo sequences for evaluation of brain parenchyma, other MRI pulse sequences or imaging options are commonly used, such as inversion recovery (short TI inversion recovery [STIR] for fat suppression, T1-weighted or T2-weighted fluid attenuated inversion recovery [FLAIR], etc.), gradient recall echo T2* imaging, spoiled gradient recall echo T1-weighted imaging, steady-state free precession imaging, magnetic transfer, diffusion/perfusion MRI, and frequency selective chemical saturation. Detailed discussions of these sequences and options can be found elsewhere.

Appearance of Abnormal Brain Parenchyma on MRI and CT

Most pathologic processes decrease the CT attenuation values of the involved tissue and increase the MRI T1 and T2 relaxation coefficients, resulting in decreased signal on T1-weighted images and increased signal on T2-weighted images relative to adjacent normal tissue. Such processes include ischemia, infarction, inflammation, infection, demyelination, dysmyelination, metabolic or toxic encephalopathy, trauma, neoplasms, gliosis, radiation injury, and

encephalomalacia-related changes. Other processes that can result in zones of low attenuation on CT include dermoids (intact or ruptured), teratomas, lipomas, and cystic structures with high protein concentration or cholesterol, as well as Pantopaque.

Areas where there is breakdown of the blood–brain barrier can be also evaluated with iodinated intravenous contrast on CT and with gadolinium-based intravenous contrast agents on MRI. Leakage of contrast agents through the blood–brain barrier results in increased attenuation on CT (contrast enhancement) and high signal on T1-weighted images. The high signal seen on MRI after contrast administration results from reduction of the T1 and T2 values of the hydrogen nuclei in brain tissue adjacent to the intraparenchymal contrast that leaked through the damaged blood–brain barrier. Contrast-enhanced CT and MR images are important portions of most imaging examinations of the head. In addition to the contrast enhancement in pathologically altered intracranial tissues, CT and MRI contrast enhancement can be seen normally in veins, the choroid plexus, the anterior pituitary gland, the pituitary infundibulum, the pineal gland, and the area postrema.

Intracranial Hemorrhage on MRI

Intraparenchymal hemorrhage on MRI can have varying appearances in the brain depending on the age of the hematoma, oxidation states of the iron in hemoglobin, hematocrit, protein concentration, clot formation and retraction, hemorrhage location, and hemorrhage size. Oxyhemoglobin in a hyperacute blood clot has ferrous iron and is diamagnetic. Oxyhemoglobin does not significantly alter the T1 and T2 values of the tissue environment, other than causing possible localized edema. After a few hours during the acute phase of the hematoma, the oxyhemoglobin loses its oxygen and forms deoxyhemoglobin. Deoxyhemoglobin also has ferrous iron, although it has unpaired electrons and becomes paramagnetic. As a result, deoxyhemoglobin shortens the T2 value of the acute clot but does not significantly change the T1 value. On MRI, deoxyhemoglobin in the clot will have an intermediate T1 signal and a low signal on T2-weighted spin echo or gradient echo images. Later, in the early subacute phase of the hematoma, deoyxhemoglobin becomes oxidized to the ferric state, methemoglobin, which is strongly paramagnetic. Methemoglobin shortens the T1 value of hydrogen nuclei, resulting in high signal on T1-weighted images. While the red blood cells in the clot are intact, with intracellular methemoglobin, the T2 values will also be decreased, resulting in a low signal on T2-weighted images. In the late subacute phase, breakdown of the membranes of the red blood cells results in extracellular methemoglobin, which causes high signal on both T1- and T2-weighted images. In the chronic phase, methemoglobin becomes further oxidized and broken down by macrophages into hemosiderin, which has a prominent low signal on T2-weighted images and a low-intermediate signal on T1-weighted images.

The MRI features of *subdural hematomas* are variable, although the appearances can progress in patterns similar to those for intraparenchymal hematomas. Chronic subdural hematomas often have a low-intermediate signal on T1-weighted images and a high signal on T2-weighted images. *Subarachnoid hemorrhage* is often difficult to see on T1- and T2-weighted images, although it can be sometimes identified on long TR/short TE (proton density-weighted images) or FLAIR images.

In the differential diagnosis of intracranial hemorrhage, other processes that can result in zones of high signal on T1-weighted images are fat, dermoids (intact or ruptured), teratomas, lipomas, and cystic structures with high protein concentration or cholesterol, as well as Pantopaque.

Intracranial Hemorrhage on CT

An *intraparenchymal hemorrhage* on CT can have varying appearances in the brain depending on the age of the hematoma, hematocrit, protein concentration, clot formation and retraction, hemorrhage location, and hemorrhage size. In the first week, intraparenchymal hematomas typically have high attenuation.

In the late subacute phase (> 7 days to 6 weeks) *intracerebral hematomas* decrease 1.5 Hounsfield units (HU) per day and become isodense to hypodense. Chronic hematomas have low attenuation with localized encephalomalacia. The CT features of *subdural hematomas* are variable, although the appearances can progress in patterns similar to those for intraparenchymal hematomas. Acute subdural hematomas often have high attenuation. CT is the optimal exam in the diagnosis of acute *subarachnoid hemorrhage* and is more reliable than MRI. Also, CT is the optimal exam to diagnose acute *epidural and subdural hematomas* because of wide scanner availability and fast imaging acquisition, as well as capability for the evaluation of commonly associated skull injuries and fractures.

Chapter 1

Brain (Intra-Axial Lesions)

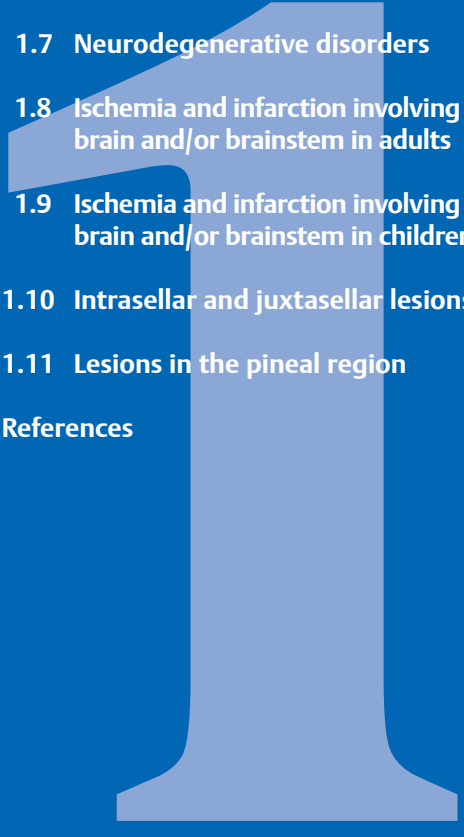

1 Brain (Intra-Axial Lesions)

Introduction

Overview of Embryonic and Fetal Brain Development

Neural Plate and Neural Tube Formation

A. Neural Plate Formation

a. At ***5 to 15 days' gestation,*** proliferating ectodermal cells on the dorsal surface of the embryo form the primitive streak (**Fig. 1.1**).

b. A group of proliferating cells at the cephalic end of the primitive streak form a pit called Hensen's node.

c. At ***15 to 16 days' gestation***, cells enter Hensen's node and migrate rostrally toward the cephalic end of the embryo to form the notochord process and eventually the notochord.

d. The notochord induces the overlying dorsal ectoderm into forming neuroectoderm, which becomes the neural plate (this is the process of *neurulation*).

e. At ***17 days' gestation***, the lateral portions of the neural plate thicken to produce the neural folds. The neural folds elevate laterally and contract centrally to form the neural groove.

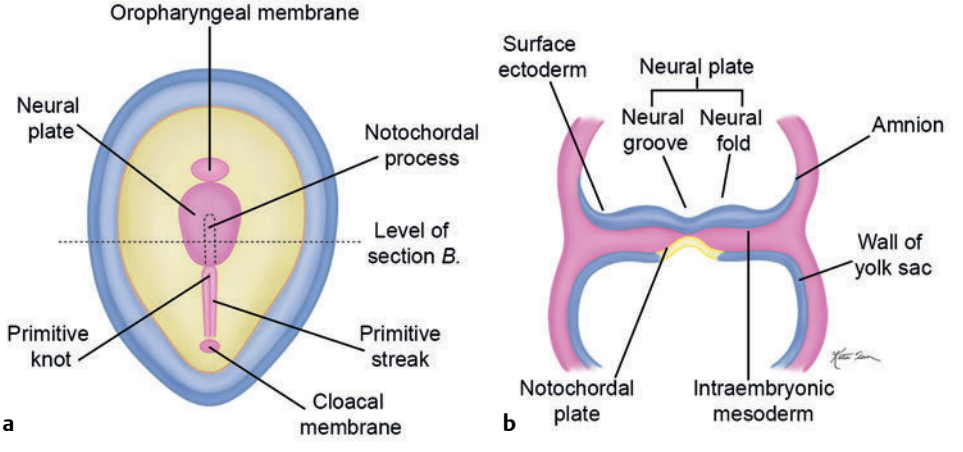

Fig. 1.1 **(a)** Dorsal and **(b)** coronal diagrams of the developing embryo.

B. Neural Tube Formation

a. At ***20 days' gestation***, the mesenchyme adjacent to the neural folds expands, in association with progressive approximation and eventual merger of neural folds in the midline dorsally to form the neural tube (**Fig. 1.2**). Progressive closure of the neural tube begins at two or three sites.

The neuroectoderm of the developing neural tube is covered by cutaneous ectoderm. Separation (*disjunction*) of the neuroectoderm and cutaneous ectoderm occurs as the neural folds fuse to form the neural tube. The neural tube forms the central nervous system, and the cutaneous ectoderm becomes the skin. Mesenchyme migrates between the separated cutaneous ectoderm and neuroectoderm to eventually form the meninges, vertebrae, and paraspinal muscles.

b. At ***25 days' gestation***, closure of the neural tube occurs at the cephalic end (anterior neuropore).

c. At ***27 to 28 days' gestation***, closure of the neural tube occurs at the caudal end (posterior neuropore).

d. Neuroectodermal cells at the lateral dorsal margins of the closing neural tube separate to form the neural crest cells.

Abnormalities of neural tube closure include cephaloceles, myeloceles, and Chiari malformations.

Vesicles

a. At ***35 days' gestation***, three fluid-filled primary expansions or vesicles form at the cephalic (rostral) end of the neural tube: the *prosencephalon, mesencephalon*, and *rhombencephalon* (**Fig. 1.3**). The prosencephalon (forebrain) will bend and constrict to form the *telencephalon* (cerebral hemispheres, basal ganglia, and lateral ventricles) and *diencephalon* (thalamus, hypothalamus, and third ventricle). The mesencephalon (midbrain) will form the midbrain and cerebral aqeduct and the rhombencephalon (hindbrain) will eventually become the metencephalon (pons, cerebellum, and upper portion of the fourth ventricle) and myelencephalon (medulla and lower portion of the fourth ventricle).

b. At ***42 days' gestation***, lateral protrusions of the prosencephalon begin formation of the cerebral hemispheres (**Fig. 1.4** and **Fig. 1.5**).

Abnormal formation of the vesicles causes the congenital cleavage anomalies, such as holoprosencephalies (alobar holoprosencephaly, semilobar holoprosencephaly, lobar holoprosencephaly, syntelencephaly), septo-optic dysplasia, and arrhinencephaly.

Neuronal Migration

a. At ***49 days' gestation to 22 weeks***, neuronal progenitor cells and stem cells arise at the innermost layer of the fetal cerebral hemisphere, which is referred to as the *ventricular zone* or *germinal zone*. At the *basal (ventral) portions* of the ventricular zone, neurons of the basal ganglia, some thalamic neurons, and GABAergic cortical interneurons develop at regional thickening of the ventricular zone, referred to as the *ganglionic germinal zone* (ganglionic eminence). This region of the ventricular germinal zone is referred to as the *subpallium*. The caudate nucleus develops at the rostral end of the ganglionic eminence. GABAergic cortical interneurons are produced in the medial ganglionic eminences of the subpallium and migrate tangentially.

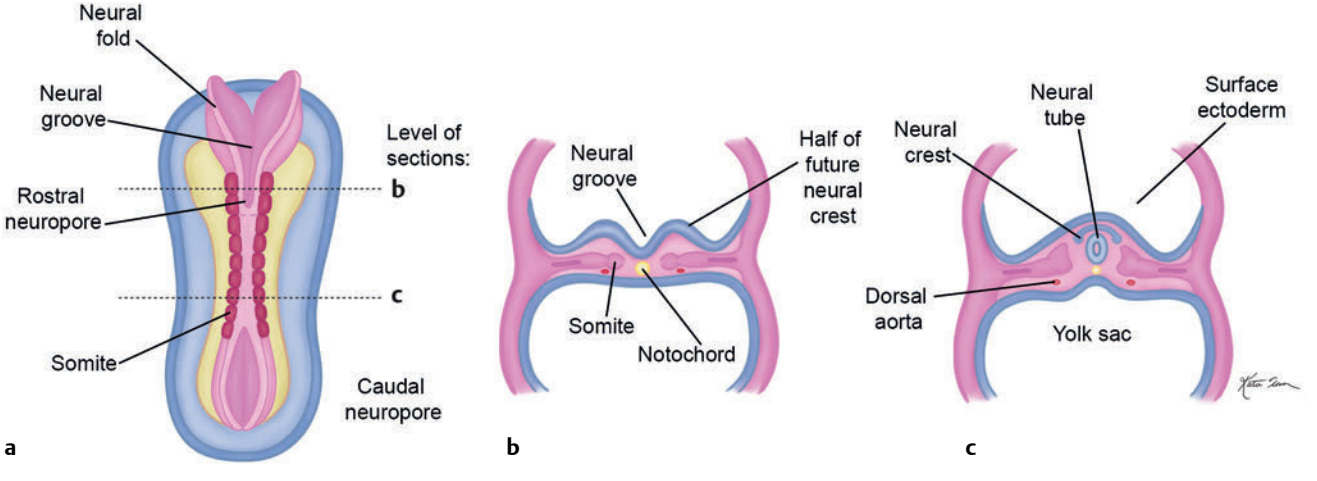

Fig. 1.2 **(a)** Dorsal view of the embryo shows closure of the neural tube, except at the rostral and caudal neuropores. **(b)** Coronal view shows infolding of the neural folds at the neural groove that eventually close to form the neural tube **(c)**.

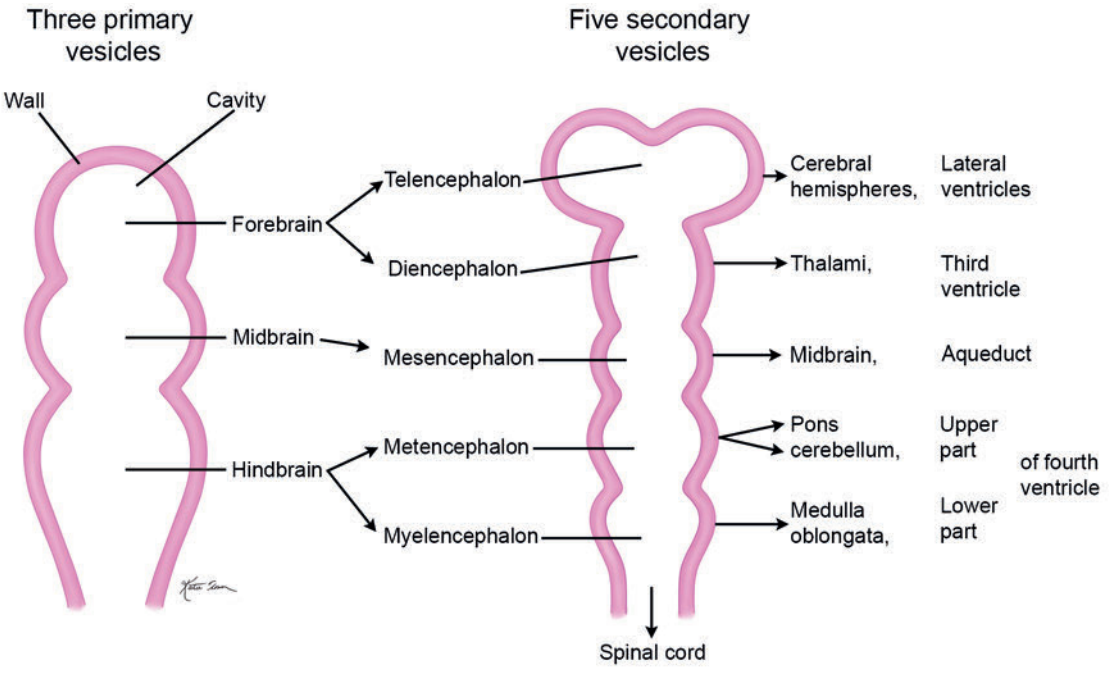

Fig. 1.3 Coronal diagram of the rostral neural tube shows initial formation of the primary vesicles, followed by the secondary vesicles and corresponding mature neural structures.

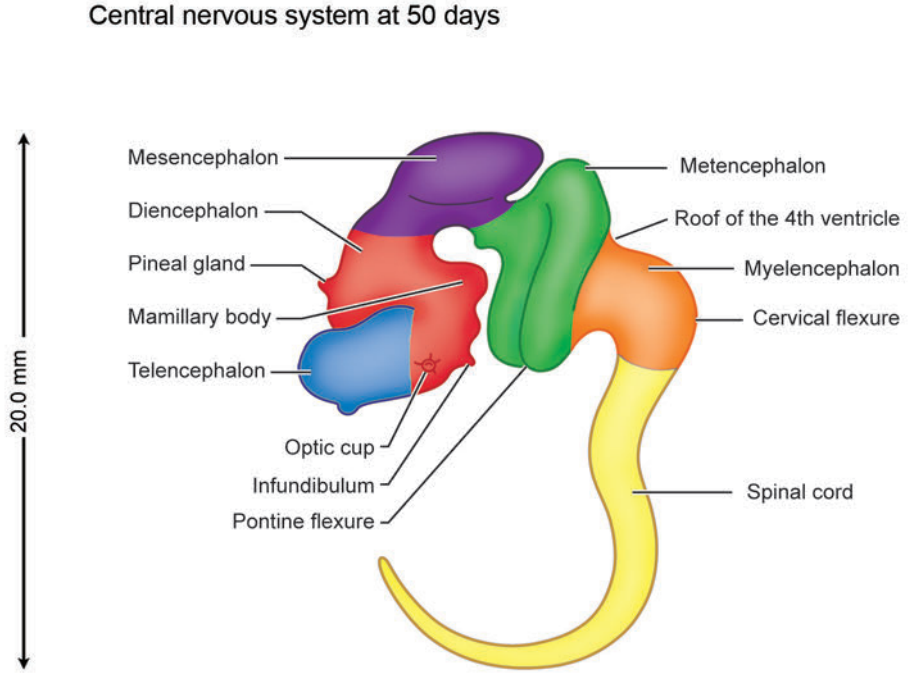

Fig. 1.4 Lateral diagram shows the CNS at 50 days' gestation.